Moiré Valleytronics: Realizing Dense Arrays of Topological Helical Channels

Chen Hu,[1,*] Vincent Michaud-Rioux,[1] Wang Yao,[2] and Hong Guo[1,3,4]
[1]Center for the Physics of Materials and Department of Physics, McGill University, Montreal, Quebec H3A 2T8, Canada
[2]Department of Physics and Center of Theoretical and Computational Physics, University of Hong Kong, Hong Kong, China
[3]Center for Computational Sciences, Sichuan Normal University, Chengdu 610066, China
[4]College of Physics and Energy, Shenzhen University, Shenzhen 518060, China

(Received 17 April 2018; published 2 November 2018)

We propose a general and robust platform, the *moiré valleytronics*, to realize high-density arrays of 1D topological helical channels in real materials at room temperature. We demonstrate the idea using a long-period 1D moiré pattern of graphene on *h*BN by first-principles calculation. Through calculating the Berry curvature and topological charge of the electronic structure associated with various local graphene/*h*BN stackings in the moiré pattern, it is revealed that the helical channel arrays originate intrinsically from the periodic modulation of the local topological orders by the moiré pattern. For a freestanding wavelike moiré pattern, two groups of helical channel arrays are spatially separated out of plane, validating the structural robustness of the moiré topology. The generality and experimental feasibility of moiré valleytronics are demonstrated by investigating a broad range of moiré systems.

DOI: 10.1103/PhysRevLett.121.186403

Two-dimensional (2D) van der Waals (vdW) heterostructures have attracted great attention in the past few years [1]. By stacking different 2D materials to weakly bond via the vdW force, the resulting artificial bilayers and/or multilayers create novel material platforms for fundamental as well as technological exploration. A nearly ubiquitous feature of the vdW heterostructures is the moiré patterns caused by lattice mismatch or the relative rotation of the two stacking lattices [1–4]. Moiré patterns can create a *periodic* lateral modulation on the electronic property in the heterostructure leading to interesting new physics. These include the appearance of secondary Dirac cones [5] and the self-similar Hofstadter butterfly states [6] in a graphene(Gr)/*h*BN bilayer, the nanoscale patterned optical properties and spin-orbit coupled exciton superlattices [7] and moiré-defined superstructures of quantum spin Hall insulators [8] in transition metal dichalcogenides, and helical networks under an interlayer bias [9], and the newly found correlated insulator behavior [10] and superconductivity [11] in a twisted graphene bilayer. Since a moiré superlattice can be experimentally created, they provide extraordinary opportunities for generating novel electronic properties that are hard to obtain otherwise.

In hexagonal 2D crystals, the *valley* degree of freedom, referring to the degenerate Bloch band extrema at K and K' corners of the hexagonal Brillouin zone, is of particular interest [12–15]. In graphene, the nontrivial topological properties of the Dirac cones at the two valleys have led to intriguing phenomena, such as the bulk topological valley current when a gap arises through inversion symmetry breaking [16–18]. In the gapped graphene system, the bulk topological properties of the valley also give rise to in-gap valley helical channels at topological line defects [19–22], analogous to the quantum spin Hall edge states, and were experimentally demonstrated in bilayer graphene [23,24]. Such valley helical modes are protected from backscattering by the large momentum space separation and can be exploited as conducting channels for quantum electronics. However, the present realizations rely on either the random local stacking faults [23] or a dual-split-gate structure that is extremely challenging to fabricate [24]. Moreover, these schemes typically host a single pair of helical channels, limiting the applicability because high-density valley channels and currents are required in circuit integration.

In this work, we propose a general and robust platform, the moiré valleytronics, to realize high-density arrays of 1D topological helical channels at room temperature and in realistic easily fabricatable materials. Specifically, a 1D graphene(Gr)/*h*BN moiré pattern and several other moiré systems are shown to establish the moiré valleytronics. For the 1D graphene(Gr)/*h*BN moiré pattern, we show by first-principles calculations that a long-period moiré pattern realizes dense arrays of helical channels inside the noncryogenic bulk gap opened by local inversion symmetry breaking due to the *h*BN. These helical channels arise from the periodical modulation in the topological order of local electronic structure, due to the variation of atomic stacking in the moiré pattern. The generality and structural robustness of moiré valleytronics are demonstrated by investigating a broad range of moiré systems and freestanding Gr/*h*BN moiré structures.

Figure 1(a) shows the orientation of the graphene and the *h*BN lattices; the latter has a lattice constant mismatch of 1.8% larger than that of the graphene. We will focus on the 1D moiré pattern (1DMP) formed by stacking graphene on

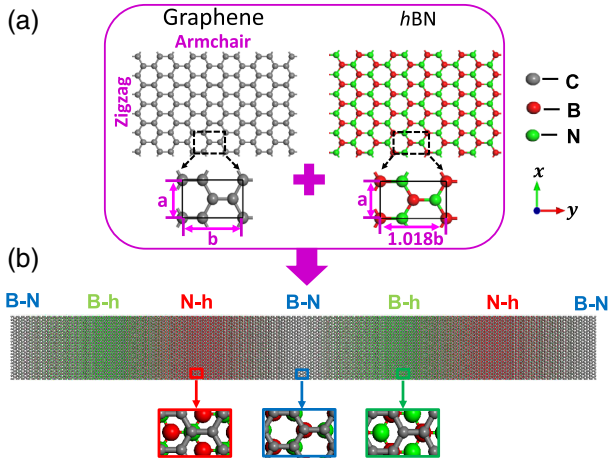

FIG. 1. (a) The graphene and *h*BN lattices, strained along the zigzag direction to match while left free along the armchair direction (insets) to form the 1D moiré pattern. a and b are the lattice constants of primitive graphene, with the value of 2.4595 and 4.26 Å, respectively. (b) The 1D moiré pattern periodic along the armchair direction formed by three different high-symmetry local stacking configurations indicated as N-*h*, B-*h*, and B-N stacking.

*h*BN along the armchair direction [see Fig. 1(a)]. To do so, *h*BN is compressed along the zigzag direction (x direction) to match the graphene, while its armchair direction (y) is left to freely and vertically stack on graphene, resulting in a periodic 1DMP shown in Fig. 1(b). Along the armchair direction, the atomic registry of the two lattices varies gradually and continuously, giving rise to the periodic appearance of three high-symmetry local stacking configurations: the carbon atoms on top of boron or nitrogen atoms (B-N), the carbon atoms on top of boron or hollow sites (B-*h*), and carbon on nitrogen and hollow sites (N-*h*); see Fig. 1(b). Each moiré period has a real space width of 238.56 Å, containing 56 graphene primitive cells stacked on 55 *h*BN primitive cells, and Fig. 1(b) shows two such moiré periods. The moiré pattern extends periodically and infinitely in the 2D x-y plane but shall be referred to as 1DMP due to its quasistripe shape along the y direction. Finally, the distance between graphene and *h*BN is 3.22 Å, which corresponds to the equilibrium distance of the most stable local stacking configuration (B-*h*) [25]. Experimentally, we note that a similar 1DMP system has been demonstrated by using strained bilayer graphene [26] (details can be seen in Supplemental Material [27]).

The electronic band structure of the 1DMP is plotted in Fig. 2(a), showing characteristic Dirac cones at the K and K' valleys. Since the two valleys are far apart in the Brillouin zone, they can serve as a new degree of freedom when describing the low-energy electronic states [12,22]. Most prominently, besides the noncryogenic bulk band gap (261.6 meV) opening due to local spatial symmetry breaking, there are two linear metallic bands near the Fermi level (red and blue lines) at each Dirac point which turn out to be

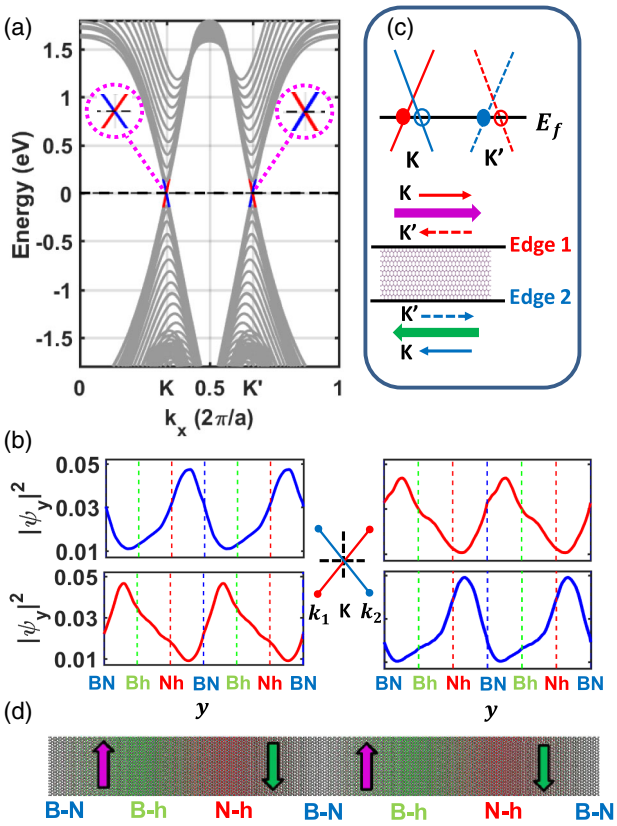

FIG. 2. (a) Band structure of the 1DMP. The linear bands near the Fermi level (energy zero)—red and blue lines—are the two valley helical channels, and the gray lines are bulk bands. The valley points K and K' are at $k_x = 1/3$ and $2/3$, respectively. (b) Wave functions $|\psi_y|^2$ along the armchair (y) direction of the two helical channels with the same color scheme; vertical dashed lines indicate central positions of the three high-symmetry local stacking configurations. The left (right) panels are for $k_1 = 0.3329$ ($k_2 = 0.3338$), located at the left (right) of the K valley. (c) Illustration of valley helical channels and valley current. Upper: Solid (empty) circles denote carriers with positive (negative) group velocity, i.e., right movers (left movers). Solid (dashed) lines are helical channels with valley index K or K', respectively. Lower: The red (blue) color is for the channels located at edge 1 (2); purple and green arrows indicate valley currents. (d) Topological valley currents flow at the moiré edges.

helical channels (see below), one with positive and the other with negative group velocity. The spatial distribution of the wave function $|\psi_y|^2$ is shown in Fig. 2(b). By tracking the peaks of $|\psi_y|^2$ near the K valley (and similarly at the K' valley), one can find that the two linear band states are periodically located on the 1DMP: One (red) is between the B-N and B-*h* stackings, while the other (blue) between N-*h* and B-N stackings. In the rest of the Letter, the peak regions of $|\psi_y|^2$ shall be named *topological moiré edges*. The property of the K' valley is easily envisioned, since wave functions at K and K' are connected by time-reversal symmetry. Figure 2(c) sketches that the helical channels can generate a pure topological valley current. At each

topological moiré edge, carriers with different valley indexes (K or K') have opposite group velocities (moving directions), leading to a pure topological valley current. Namely, at different edges the valley current propagates oppositely. Figure 2(d) illustrates two groups of topological valley current flowing oppositely at the moiré edges. Analogous to the spin-dependent helical states in a quantum spin Hall system [8,37], the valley current is quantized and topologically robust against small chemical potential variations. Interestingly and importantly, in contrast with most previous schemes where only a single topological edge can be found or created at the boundary of the crystals, the periodic 1DMP can, in principle, support dense arrays of such topological moiré edges, with an integrated density of two per moiré period (238.56 Å). Thus, multiple helical channels can be implemented periodically and simultaneously, which is greatly beneficial for applications in quantum electronics and high-density integrated circuits.

To establish the topological nature and origin of the helical channels of 1DMP in Fig. 2(a), we analyze the topological properties of the electronic structures in the 1DMP. In a long-period moiré pattern with the period much larger than the lattice constant in graphene, the electronic structures in a local region, with the length scale small compared to the moiré period but large compared to the lattice constant, can be approximated by that of the lattice-matched Gr/hBN of the corresponding atomic registry. The topological nature of the latter can be quantified by the Berry curvature $\mathbf{\Omega}(\mathbf{k})$ using the Kubo formula [38–40]:

$$\mathbf{\Omega}_{n,xy}(\mathbf{k}) = -2\mathrm{Im}\sum_{m\neq n}\frac{\langle\psi_{n\mathbf{k}}|v_x|\psi_{m\mathbf{k}}\rangle\langle\psi_{m\mathbf{k}}|v_y|\psi_{n\mathbf{k}}\rangle}{[\epsilon_{m\mathbf{k}}-\epsilon_{n\mathbf{k}}]^2}, \quad (1)$$

where m and n are the band indices, $\epsilon_{\mathbf{k}}$ is the eigenvalue of the eigenstate $|\psi_{\mathbf{k}}\rangle$, and v_x and v_y are the components of velocity operators. As shown in Fig. 3(b), for every lattice-matched configuration, the Berry curvature $\mathbf{\Omega}(\mathbf{k})$ of the conduction band is strongly concentrated at the valley point with the equal amplitude but opposite sign for K and K'. Comparing the three panels, one can find two types of $\mathbf{\Omega}$ polarity: $\mathbf{\Omega}$ of the K valley is negative for the B-N stacking (middle panel) but positive for the other two. Because of the interlayer interactions from the hBN layer, the graphene sublattice obtains a finite staggered on-site potential Δ. Various local stackings give rise to different signs of Δ, which further lead to different $\mathbf{\Omega}$ polarities. More details can be found in Supplemental Material [27]. Furthermore, the topological charge $\tilde{N}_3$—a physical indicator which is often used to classify topological phases—can be obtained from the flux of the 2D Berry curvature:

$$\tilde{N}_3 = \frac{1}{2\pi}\int \mathbf{\Omega}_{xy}(\mathbf{k})d\mathbf{k_x}d\mathbf{k_y}. \quad (2)$$

In the Gr/hBN bilayer, the total $\tilde{N}_3$ of the band is zero, since $\mathbf{\Omega}(\mathbf{k}) = -\mathbf{\Omega}(-\mathbf{k})$ protected by time-reversal symmetry. Nevertheless, one can define a valley topological charge for each valley [12,22]. Figure 3(c) plots the valley topological phase diagram, showing how the topological charge $\tilde{N}_3$ of the K valley varies with the atomic registry. Clearly, there are two topological phase transitions when the atomic registry varies by one period.

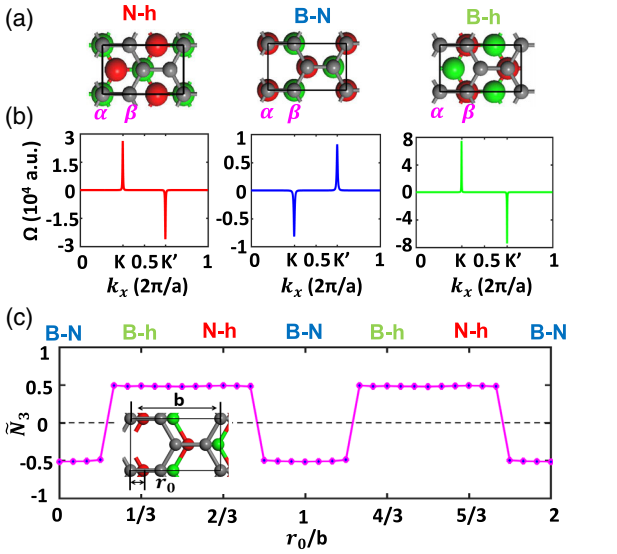

FIG. 3. Topology analysis of the lattice-matched Gr/hBN bilayer. (a) Three high-symmetry stacking configurations in the moiré structure, where α and β are two subsites of the graphene lattice. (b) Corresponding k-resolved Berry curvature $\Omega(k)$ of the linear conducting band. (c) Valley-dependent topological phase diagram parametrized by r_0, which is the lattice displacement between Gr and hBN layers, and $\tilde{N}_3$ is the calculated topological charge of the K valley.

The helical channels and topological valley current anticipated in Fig. 2(d) are the direct manifestation of the topological phase transitions by the variation of the atomic registry. The topological moiré edges in Fig. 2(d) are fully consistent with the phase transition points shown in Fig. 3(c). This picture is corroborated by the bulk-edge correspondence analysis in Supplemental Material [27]. For 1DMP, the moiré period (238.56 Å) is much greater than the lattice constant (4.26 Å); therefore the local atomic configuration varies so slowly that it has a negligible difference from lattice-matched structures. Previous studies have shown that the *local* electronic property can be described quite well by using the lattice-matched stackings in Gr/hBN [41]. From this point of view, one can track the local topological properties of the moiré superlattice according to the topological phase diagram of the lattice-matched stackings in Fig. 3(c). Along the direction of the moiré superlattice (y in our case), two local topological phases appear alternately and periodically, giving rise to two groups of "boundaries" where topological phase transitions happen, which further lead to the arrays of valley-dependent helical channels (or the topological moiré edges) in Fig. 2.

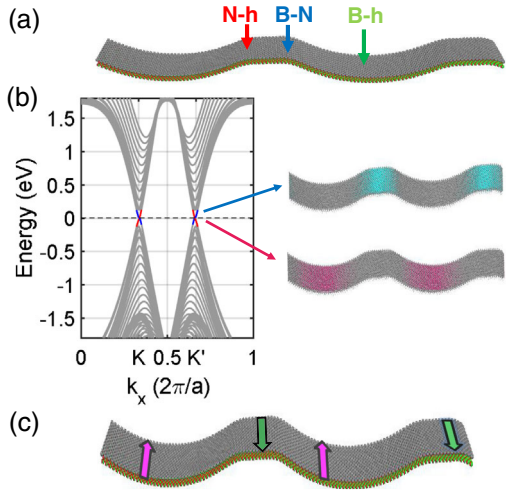

FIG. 4. (a) Relaxed freestanding Gr/hBN bilayer with out-of-plane (z-direction) corrugation of about 13 Å. (b) Left: Band structure; right: spatial distribution of modular squared wave functions of the two helical channels, where the plotted isosurface (pink and light blue areas) is 4×10^{-9} a.u. (c) Topological valley current in the freestanding moiré structure.

The key for realizing moiré valleytronics and dense arrays of 1D helical channels is a moiré structure (1DMP) that has different local stacking configurations with different topological orders. That is, different local topological phases coexist in one long-period moiré superlattice simultaneously. This situation is widely available in a broad range of 2D materials besides the Gr/hBN. In Supplemental Material [27], we demonstrate that two different real material systems possess moiré valleytronics: the strained bilayer-graphene moiré pattern and the silicence/hBN moiré pattern, where multiple moiré edges supporting dense arrays of helical channels exist between different local stackings. As mentioned above, 1DMP has been experimentally realized in strained bilayer graphene [26]; therefore 1DMP of Gr/hBN should be experimentally very realistic. To obtain a small uniaxial strain, using a polyethylene terephthalate substrate is experimentally effective [42].

In the following, we turn to another situation which could happen experimentally: the freestanding Gr/hBN moiré superlattice. By freestanding, the bilayer can fluctuate into the third dimension (z), thus changing the local stacking distribution. We determine the atomic structure of freestanding bilayers using the force-field method as implemented in the large-scale atomic/molecular massively parallel simulator (LAMMPS) [43]. In the relaxation, the vdW interaction between the two layers is well described by the optimized Morse potential (see Supplemental Material [27]). As shown in Fig. 4(a), the freestanding bilayer is 3D wavelike with a large out-of-plane corrugation (>13 Å). This corrugation originates from an energetic competition between maximizing the favorable stacking configuration (B-h) and minimizing the elastic energy of the lattice. By out-of-plane deformation, the area of B-h stacking is enlarged and pushed to the bottom of the corrugated structure, while the N-h and B-N stackings are reduced and pushed to the top location [41,44]. Experimentally, this 3D wavelike moiré structure is realized on the suspended bilayer [44]. Figure 4(b) shows that in the 3D wavelike bilayer the valley-dependent helical channels still appear in the band structure, and the wave functions of the helical channels [right panel in Fig. 4(b)] show that the two groups of helical channel arrays are vertically separated. As a consequence, the two groups of counterpropagating topological valley currents can flow at different heights in the corrugated bilayer as shown in Fig. 4(c), leading to an extra dimension to manipulate and detect the helical states. Most of all, this result shows the robustness of the topological moiré edges against a huge structural corrugation, making possible the practical applications of the proposed moiré valleytronics in fluctuated 2D systems (such as Refs. [26,44]) besides the flat ones.

In summary, we report a general and robust scheme, the moiré valleytronics, to realize dense arrays of 1D topological helical channels. For the 1DMP of a zigzag-oriented Gr/hBN bilayer, first-principles calculation shows that the two groups of helical states are located at two groups of topological moiré edges, one located between the B-N and B-h stackings while the other is between the N-h and B-N stackings. A topological phase diagram based on the calculations of Berry curvature and topological charge reveals the intrinsic dependence between the topological order and the atomic stacking configuration. Moreover, the generality and experimental feasibility have been discussed and proved by investigating broad moiré systems. Finally, we predict that, in the freestanding wavelike moiré structure, two groups of moiré edge arrays carrying counterpropagating helical channels are spatially separated in the out-of-plane direction, which proves the structural robustness of moiré valleytronics. This study paves a new way for modulating valley electronic states and realizing multiple topological helical channels using moiré patterns which are relatively easily accessible experimentally. The results suggest that valleytronics based on moiré patterns, i.e., "moiré valleytronics," to be a rich research direction in material science.

C. H. thanks Maoyuan Wang for discussion on the Berry curvature calculation and Ying-Chih Chen for providing optimized atomic basis and pseudopotentials. This work is financially supported by the Natural Science and Engineering Research Council (NSERC) of Canada (H. G.). W. Y. acknowledges support by Research Grants Council of Hong Kong (HKU17302617). We thank Compute Canada and the High Performance Computing Center of McGill University for substantial computational support which made this work possible.

*huchen@physics.mcgill.ca

[1] A. K. Geim and I. V. Grigorieva, Van der Waals heterostructures, Nature (London) **499**, 419 (2013).

[2] C. R. Woods *et al.*, Commensurate-incommensurate transition in graphene on hexagonal boron nitride, Nat. Phys. **10**, 451 (2014).

[3] S. Dai, Y. Xiang, and D. J. Srolovitz, Twisted bilayer graphene: Moiré with a twist, Nano Lett. **16**, 5923 (2016).

[4] G. T. de Laissardiere, D. Mayou, and L. Magaud, Localization of Dirac electrons in rotated graphene bilayers, Nano Lett. **10**, 804 (2010).

[5] E. Wang *et al.*, Gaps induced by inversion symmetry breaking and second-generation Dirac cones in graphene/hexagonal boron nitride, Nat. Phys. **12**, 1111 (2016).

[6] B. Hunt *et al.*, Massive Dirac fermions and Hofstadter butterfly in a van der Waals heterostructure, Science **340**, 1427 (2013).

[7] H. Yu, G. B. Liu, J. Tang, X. Xu, and W. Yao, Moiré excitons: From programmable quantum emitter arrays to spin-orbit-coupled artificial lattices, Sci. Adv. **3**, e1701696 (2017).

[8] Q. Tong, H. Yu, Q. Zhu, Y. Wang, X. Xu, and W. Yao, Topological mosaics in moire superlattices of van der Waals heterobilayers, Nat. Phys. **13**, 356 (2017).

[9] P. San-Jose and E. Prada, Helical networks in twisted bilayer graphene under interlayer bias, Phys. Rev. B **88**, 121408 (2013).

[10] Y. Cao *et al.*, Correlated insulator behaviour at half-filling in magic-angle graphene superlattices, Nature (London) **556**, 80 (2018).

[11] Y. Cao, V. Fatemi, S. Fang, K. Watanabe, T. Taniguchi, E. Kaxiras, and P. Jarillo-Herrero, Unconventional superconductivity in magic-angle graphene superlattices, Nature (London) **556**, 43 (2018).

[12] D. Xiao, W. Yao, and Q. Niu, Valley-Contrasting Physics in Graphene: Magnetic Moment and Topological Transport, Phys. Rev. Lett. **99**, 236809 (2007).

[13] X. Xu, W. Yao, D. Xiao, and T. F. Heinz, Spin and pseudospins in layered transition metal dichalcogenides, Nat. Phys. **10**, 343 (2014).

[14] C. Hu, W. Lu, W. Ji, G. Yu, Y. Yan, and J. Teng, Switchable valley injection into graphene, Phys. Rev. B **92**, 115404 (2015).

[15] M. Wang, L. Liu, C. Liu, and Y. Yao, van der Waals heterostructures of germanene, stanene, and silicene with hexagonal boron nitride and their topological domain walls, Phys. Rev. B **93**, 155412 (2016).

[16] R. V. Gorbachev *et al.*, Detecting topological currents in graphene superlattices, Science **346**, 448 (2014).

[17] M. Sui *et al.*, Gate-tunable topological valley transport in bilayer graphene, Nat. Phys. **11**, 1027 (2015).

[18] Y. Shimazaki , M. Yamamoto, I. V. Borzenets, K. Watanabe, T. Taniguchi, and S. Tarucha, Generation and detection of pure valley current by electrically induced Berry curvature in bilayer graphene, Nat. Phys. **11**, 1032 (2015).

[19] I. Martin, Y. M. Blanter, and A. F. Morpurgo, Topological Confinement in Bilayer Graphene, Phys. Rev. Lett. **100**, 036804 (2008).

[20] Z. Qiao, J. Jung, Q. Niu, and A. H. MacDonald, Electronic highways in bilayer graphene, Nano Lett. **11**, 3453 (2011).

[21] F. Zhang, A. H. MacDonald, and E. J. Mele, Valley Chern numbers and boundary modes in gapped bilayer graphene, Proc. Natl. Acad. Sci. U.S.A. **110**, 10546 (2013).

[22] W. Yao, S. A. Yang, and Q. Niu, Edge States in Graphene: From Gapped Flat-Band to Gapless Chiral Modes, Phys. Rev. Lett. **102**, 096801 (2009).

[23] L. Ju *et al.*, Topological valley transport at bilayer graphene domain walls, Nature (London) **520**, 650 (2015).

[24] J. Li, K. Wang, K. J. McFaul, Z. Zern, Y. Ren, K. Watanabe, T. Taniguchi, Z. Qiao, and J. Zhu, Gate-controlled topological conducting channels in bilayer graphene, Nat. Nanotechnol. **11**, 1060 (2016).

[25] G. Giovannetti, P. A. Khomyakov, G. Brocks, P. J. Kelly, and J. van den Brink, Substrate-induced band gap in graphene on hexagonal boron nitride: *Ab initio* density functional calculations, Phys. Rev. B **76**, 073103 (2007).

[26] J. Lin, W. Fang, W. Zhou, A. R. Lupini, J. C. Idrobo, J. Kong, S. J. Pennycook, and S. T. Pantelides, AC/AB stacking boundaries in bilayer graphene, Nano Lett. **13**, 3262 (2013).

[27] See Supplemental Material at http://link.aps.org/supplemental/10.1103/PhysRevLett.121.186403 for the $\mathbf{\Omega}$ polarity analysis, moiré valleytronics in strained bilayer graphene, moiré valleytronics in silicene/*h*BN, bulk-edge correspondence in lattice-matched stackings, armchair-oriented 1D moiré pattern, the computational details of the electronic structures, and the parameters of the moiré structure relaxations by force-field calculation, which includes Refs. [28–36].

[28] Y. Fan, M. Zhao, Z. Wang, X. Zhang, and H. Zhang, Tunable electronic structures of graphene/boron nitride heterobilayers, Appl. Phys. Lett. **98**, 083103 (2011).

[29] L. Jiang *et al.*, Soliton-dependent plasmon reflection at bilayer graphene domain walls, Nat. Mater. **15**, 840 (2016).

[30] S. Balendhran, S. Walia, H. Nili, S. Sriram, and M. Bhaskaran, Elemental analogues of graphene: Silicene, germanene, stanene, and phosphorene, Small **11**, 640 (2015).

[31] V. Michaud-Rioux, L. Zhang, and H. Guo, RESCU: A real space electronic structure method, J. Comput. Phys. **307**, 593 (2016).

[32] Y. Zhou, Y. Saad, M. L. Tiago, and J. R. Chelikowsky, Parallel self-consistent-field calculations via Chebyshev-filtered subspace acceleration, Phys. Rev. E **74**, 066704 (2006).

[33] D. R. Hamann, Optimized norm-conserving Vanderbilt pseudopotentials, Phys. Rev. B **88**, 085117 (2013).

[34] J. P. Perdew, J. A. Chevary, S. H. Vosko, K. A. Jackson, M. R. Pederson, D. J. Singh, and C. Fiolhais, Atoms, molecules, solids, and surfaces: Applications of the generalized gradient approximation for exchange and correlation, Phys. Rev. B **46**, 6671 (1992).

[35] J. Tersoff, Modeling solid-state chemistry: Interatomic potentials for multicomponent systems, Phys. Rev. B **39**, 5566 (1989).

[36] J. Tersoff, New empirical approach for the structure and energy of covalent systems, Phys. Rev. B **37**, 6991 (1988).

[37] M. Z. Hasan and C. L. Kane, Colloquium: Topological insulators, Rev. Mod. Phys. **82**, 3045 (2010).

[38] D. Xiao, M. C. Chang, and Q. Niu, Berry phase effects on electronic properties, Rev. Mod. Phys. **82**, 1959 (2010).

[39] X. Wang, J. R. Yates, I. Souza, and D. Vanderbilt, *Ab initio* calculation of the anomalous Hall conductivity by Wannier interpolation, Phys. Rev. B **74**, 195118 (2006).

[40] M. Gradhand, D. V. Fedorov, F. Pientka, P. Zahn, I. Mertig, and B. L. Györffy, First-principle calculations of the Berry curvature of Bloch states for charge and spin transport of electrons, J. Phys. Condens. Matter **24**, 213202 (2012).

[41] C. Hu, V. Michaud-Rioux, X. Kong, and H. Guo, Dirac electrons in Moiré superlattice: From two to three dimensions, Phys. Rev. Mater. **1**, 061003(R) (2017).

[42] Z.-H. Ni, T. Yu, Y. H. Lu, Y. Y. Wang, Y. P. Feng, and Z. X. Shen, Uniaxial strain on graphene: Raman spectroscopy study and band-gap opening, ACS Nano **2**, 2301 (2008).

[43] S. Plimpton, Fast parallel algorithms for short-range molecular dynamics, J. Comput. Phys. **117**, 1 (1995).

[44] G. Argentero, A. Mittelberger, M. Reza Ahmadpour Monazam, Y. Cao, T. J. Pennycook, C. Mangler, C. Kramberger, J. Kotakoski, A. K. Geim, and J. C. Meyer, Unraveling the 3D atomic structure of a suspended graphene/hBN van der Waals heterostructure, Nano Lett. **17**, 1409 (2017).